



Analytic formulas for apparent magnitude and count rate of stars in Roman pass bands using spectro-photometric information.

Sanjib Sharma[†], William C. Schultz[†]
23 December 2025

ABSTRACT

The Wide-Field Instrument (WFI) of Roman does imaging from 0.48 to 2.3 μm spanning 8 photometric bands and spectroscopy from 0.8 to 1.9 μm . The Roman telescope will use the WFI for guiding. The Fine Guidance system of the telescope needs an estimate of the flux of a star that is used for guiding and also of neighboring stars to estimate flux contamination. To support guiding, we develop easy to use analytical models to estimate the apparent magnitude and count rates in different Roman bands based on the available spectro-photometric information. Our best model makes use of BP and RP photometry, extinction, and parallax from Gaia DR3 and metallicity from the external `xgboost` catalog. The model predictions have a root-mean-square uncertainty of 0.01 mag for the bluer bands and 0.04 mag for the redder bands. The prediction uncertainty is found to increase with extinction, suggesting that one should restrict to low extinction stars for high accuracy. We show that there are sufficient stars all over the sky that have `xgboost` stellar parameters and have low extinction to serve as guide stars. Beyond guiding, the presented models should also be useful for other studies that require the use of Roman magnitudes, either in simulations involving synthetic catalog or real catalogs like Gaia and 2MASS.

^{††} Equal contribution

1 INTRODUCTION

Guide stars are essential for pointing and guiding the telescopes and for Roman this is handled by its Fine Guidance system (FGS). Unlike other telescopes that have a separate guiding camera, the FGS uses the Roman’s imaging instrument, the Wide-Field Instrument (WFI), for guiding. The WFI aboard Roman is designed to do imaging from 0.48 to 2.3 μm spanning 8 photometric bands and spectroscopy from 0.8 to 1.9 μm . A set of predefined pixels are identified on the WFI for the purpose of guiding and are known as the guide window. A minimum of 4 and a maximum of 18 guide stars are required for guiding and a detector is not allowed to have more than one guide star. The guide stars should be bright enough to be observed in a given exposure time and faint enough to not saturate the detector in that exposure time. Additionally, once a guide star has been located, we need to check if it is the correct guide stars by comparing its observed count rates to that of predicted count rates. This necessitates that we predict the apparent magnitude or count rates of a guide star in a bandpass the telescope is going to observe, and this is the main focus of this document. For spectroscopic guiding the FGS uses a blackbody spectrum corresponding to the temperature of a star as a model spectrum and fits it to the observed data in the guide window. To facilitate this we discuss the use of spectroscopic stellar parameters.

A brief description of the FGS and the process of selecting guide stars were described in [Reinhart \(2022\)](#). Algorithms to predict the apparent magnitude and count rates for stars based on their photometric information in an input catalog were presented in [Reinhart \(2023\)](#). This provides a good starting point but the accuracy and precision of the predicted count rates can be further improved and this is the main focus of this study. We begin by summarizing the work done by [Reinhart \(2023\)](#) and then present our new approach. Python package describing our implementation is publicly available ², also is available codes that were used to create the data files that are used in the package ³.

2 METHODS

2.1 Basic formalism

The basic formalism that we follow is based on the work of [Reinhart \(2023\)](#), where the apparent magnitude m_R of a star in a Roman bandpass ([Figure 1](#)) was expressed as a function of apparent magnitudes in some existing bandpasses, m_{B1} and m_{B2} , by the following functional form

$$m_R = m_{B1} + c_0 + c_1x + c_2x^2 + c_3x^3 + c_4x^4. \quad (1)$$

Here c is a set of polynomial coefficients, $x = P(m_{B1} - m_{B2})$ is a color based on magnitudes m_{B1} and m_{B2} and P is parity which can be chosen to be either -1 or 1. In other words a given photometric color, $m_R - m_{B1}$ (with a band we are interested in), was expressed as a fourth order polynomial of another color x . The coefficients c were determined by fitting to a set of 2670 stars from open cluster M35 with known values of m_R , m_{B1} and m_{B2} . The m_{B1} and m_{B2} were taken from a photometric catalog and are observed magnitudes, the m_R was estimated using the

²<https://github.com/sanjibs/roman-magnitudes>

³<https://stsci.box.com/s/s2747wri7meapblsp5wi596yo5wr3zp7>

Pickles library of synthetic stellar spectra. Stellar spectra for various different values of extinction $E = E_{B-V}$ were generated. These spectra were then used to estimate photometric magnitudes in Roman, SDSS, 2MASS and *Gaia* bands. For a given star in the training set, the observed multi-band photometry in the (g, r, i, z, J, H, K_s) bands was used to determine the best fit stellar template S_k and the value of extinction E .

While the above approach for estimating the Roman magnitudes works, there are areas which can be improved upon.

1. The color-color relations are not universal. In general, such relations have a dependence on extinction, metallicity and luminosity class (or surface gravity) of a star. The cluster M35 has a metallicity of $[\text{Fe}/\text{H}] = -0.21$ and has high extinction $A_V \sim 1.64$, both of which are not representative of the stars we are interested in. Hence by choosing stars in M35 as our training set, we are not only losing precision, but are also biasing our estimates of apparent magnitudes.
2. The stars in the training set are in general very faint (by 2MASS and *Gaia* standards), median G_{BP} being 17.9 mag and median J being 15.5 mag, and consequently have large photometric uncertainties, which will decrease the accuracy of the derived Roman magnitudes.
3. Multi-band photometry in bands (g, r, i, z, J, H, K_s) is not enough to reliably estimate both the extinction and stellar parameters. This will lead to imprecise estimates of Roman magnitudes in the training set.
4. The stellar template library used is less than ideal for a number of reasons. First, it has only 131 templates, so the sampling of the $(T_{\text{eff}}, \log g)$ parameter space is very coarse. Second, the templates have no metallicity dependence. Third, templates have a wavelength resolution of 5 Å, which is too large. Finally, in roughly half of the spectral templates, the near infrared region is approximated by a black body and hence lacks the absorption lines and features that are seen in real spectra.

2.2 New improved approach

To address the shortcomings raised in [subsection 2.1](#), we make a number of changes. First, we introduce a dependence on absolute magnitude. Second, we introduce a dependence on extinction A_G and metallicity $[\text{M}/\text{H}]$. The extinction A_G is taken from *Gaia* DR3 (`ag_gspphot`) and metallicity $[\text{M}/\text{H}]$ from the *Gaia* `external.xgboost` catalog (`mh_xgboost`).

The dependence on absolute magnitude is handled indirectly through a parameter called f_{giant} , which represents the probability of a star being a giant (as opposed to a dwarf) based on its photometry. Relations for dwarfs and giants are derived separately and the parameter f_{giant} is used to appropriately weigh the two relations to arrive at the final estimate of apparent magnitudes. f_{giant} is defined by a line in $(M_{G_{RP}}, G_{BP} - G_{RP})$ plane as given by

$$M_{G_{RP}, \text{giant}} = k_0 + k_1(G_{BP} - G_{RP}), \quad (2)$$

with $k_0 = 0$ and $k_1 = 1.41$. In fact, k_1 is defined in terms of extinction coefficients as $k_1 = A_{G_{RP}} / (A_{G_{BP}} - A_{G_{RP}}) \sim 1.41$, so that the classification line is parallel to the extinction vector and

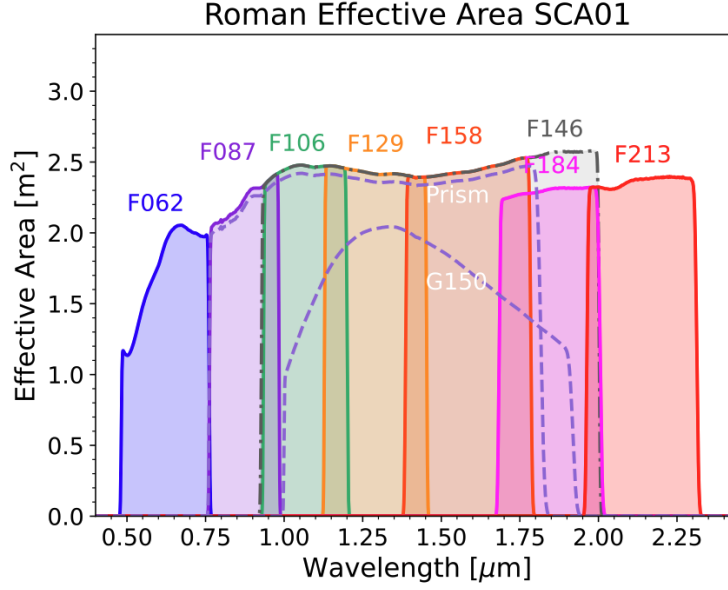


Figure 1: Effective area curves for different Roman bandpasses. Source: https://roman.gsfc.nasa.gov/science/WFI_technical.html

remains unaffected by it. This works because the extinction vector in an HR diagram is approximately parallel to the main sequence (see Figure 4). The relative contribution of giant-based vs dwarf-based relation is controlled by a tanh function (which is good for modeling smooth changes) as given by

$$f_{\text{giant}} = \frac{1}{2} \left(1 + \tanh \left(\frac{M_{G_{\text{RP,giant}}} - M_{G_{\text{RP},\omega}}}{0.5} \right) \right), \quad (3)$$

where

$$M_{G_{\text{RP},\omega}} = m_{G_{\text{RP}}} - 5 \log \left(\frac{100 \text{ mas}}{\omega} \right), \quad (4)$$

is absolute magnitude based on parallax ω . The distinction between giants and dwarfs combine with the addition of extinction, A_G , to generate more accurate apparent Roman magnitudes, $m_{R,l}$.

For a class of stars $l \in \{\text{giant, dwarf, none}\}$, $m_{R,l}$ is given by a multivariate polynomial of the form

$$m_{R,l} = m_{B1,l} + c_{0,l} + c_{1,l} x + c_{2,l} x^2 + c_{3,l} x^3 + c_{4,l} x^4 + c_{5,l} [\text{M}/\text{H}] + c_{6,l} A_G + c_{7,l} A_G^2 + c_{8,l} A_G x, \quad (5)$$

If f_{giant} is known, the dwarf and giant apparent magnitude estimates can be combined to estimate the final apparent magnitude, otherwise, a third set of coefficients can be used

$$m_R = \begin{cases} m_{R,\text{giant}} f_{\text{giant}} + m_{R,\text{dwarf}} (1 - f_{\text{giant}}), & \text{if } f_{\text{giant}} \text{ is known} \\ m_{R,\text{none}}, & \text{otherwise} \end{cases} \quad (6)$$

Note, we also experimented with adding absolute magnitude explicitly as an extra feature in the regression model, but did not find any extra improvement in the estimation of Roman magnitudes.

2.3 The Guide star catalog and the new updates to it

The Roman mission will make use of the the Guide Star Catalog ([Lasker et al. 2008](#), [GSC](#),) as the input catalog for selecting guide stars. The GSC was originally constructed to support the pointing and target acquisition of the Hubble Space Telescope but has since been adopted for numerous other purposes. The current version is based on sources from *Gaia* DR3 which provides photometry in the optical G ($0.673 \mu\text{m}$), G_{BP} ($0.532 \mu\text{m}$) and G_{RP} ($0.797 \mu\text{m}$) bands ([Gaia Collaboration et al. 2023](#)). The GSC is cross-matched to the Two-Micron-All-Sky-Survey (2MASS, [Skrutskie et al. 2006](#)) which provides photometry in the near infrared bands J ($1.25 \mu\text{m}$), H ($1.65 \mu\text{m}$) and Ks ($2.15 \mu\text{m}$) bands⁴. This is important given that the focus of the Roman mission is near infrared bands. The GSC also offers mid-infrared photometry by cross-matching with the WISE survey (bands W_1 , W_2 , W_3 and W_4). Photometry is also available in other bands, e.g., APASS ([Henden et al. 2015](#)), SDSS ([Aihara et al. 2011](#)), and PanSTARRS ([Flewelling et al. 2020](#)), but we ignore them here as they are either shallower than *Gaia* or are not available over the whole sky. Hence we can redefine our problem to predict the apparent magnitude of a star in Roman bands given the information available about that star in *Gaia* DR3 and 2MASS surveys.

With *Gaia* DR3 we now have low resolution prism based spectra in two bands named BP and RP, collectively known as *Gaia* XP spectra ([De Angeli et al. 2023](#)), and some studies have derived stellar parameters making use of them. In fact GSCv3.2 now includes WISE band photometry W_1 , W_2 from CatWISE2020 catalog ([Marocco et al. 2021](#)), stellar parameters from *Gaia* RVS (radial velocity spectrometer that gives near infrared spectra with resolution of $R = 11500$) ([Katz et al. 2023](#)), and stellar parameters from *Gaia* XP spectra both by the `xgboost` pipeline of [Andrae et al. \(2023b\)](#) and the pipeline by [Zhang et al. \(2023\)](#).

Stellar parameters derived from XP spectra were released in *Gaia* DR3. However, various third party catalogs of stellar parameters based on XP spectra have also been constructed and released. One such promising catalog is by [Andrae et al. \(2023a\)](#), which uses the `xgboost` algorithm trained on stellar parameters from the APOGEE high resolution spectroscopic survey. In addition to XP spectra and *Gaia* photometry they also make use of CatWISE photometry in W_1 and W_2 bands, which is essential to reduce the degeneracy between T_{eff} and extinction. The catalog provides estimates of surface gravity $\log g$, effective temperature T_{eff} and metallicity [M/H] for ~ 175 million stars. Another catalog based on XP spectra is by [Zhang et al. \(2023\)](#), which provides stellar parameters for ~ 220 million stars. They make use of XP spectra, G , G_{BP} , G_{RP} photometry from *Gaia*, J , H , Ks photometry from 2MASS and W_1 , W_2 from unWISE ([Schlafly et al. 2019](#)). They train the model based on stellar parameters from LAMOST. As compared to [Andrae et al. \(2023a\)](#), in addition to having more stars, [Zhang et al. \(2023\)](#) also provide estimates of extinction and uncertainties on estimated stellar parameters. We tested both catalogs, and found them to be equally good at predicting the Roman magnitudes. However, in this report we make use of the [Andrae et al. \(2023a\)](#) catalog as it provided slightly lower uncertainties in the estimated Roman magnitudes.

⁴The 2MASS is in general shallower than *Gaia*. However, since extinction is stronger in optical bands, the GSC might be missing some 2MASS stars in regions with high extinction

Table 1: Percentage of sky with density ρ of guide stars less than a given threshold for various different catalog. ρ is measured in number of stars per 0.32 square degree (the area of the bounding box of Roman WFI)

Catalog	Magnitude	Extinction	Missing Sky % $\rho < 20$	Missing Sky % $\rho < 10$	Missing Sky % $\rho < 5$
2MASS	$10 < K_s < 13$		0.002	0	0
2MASS	$10 < K_s < 14$		0.0	0	0
GSPSPEC			36	4	0.022
XGBOOST	$10 < G < 17$	$A_G < 10$	0.096	0.026	0.026
XGBOOST	$10 < G < 17$	$A_G < 1.0$	0.5	0.24	0.1
XGBOOST	$10 < G < 17$	$A_G < 0.5$	2.8	1.7	1.0

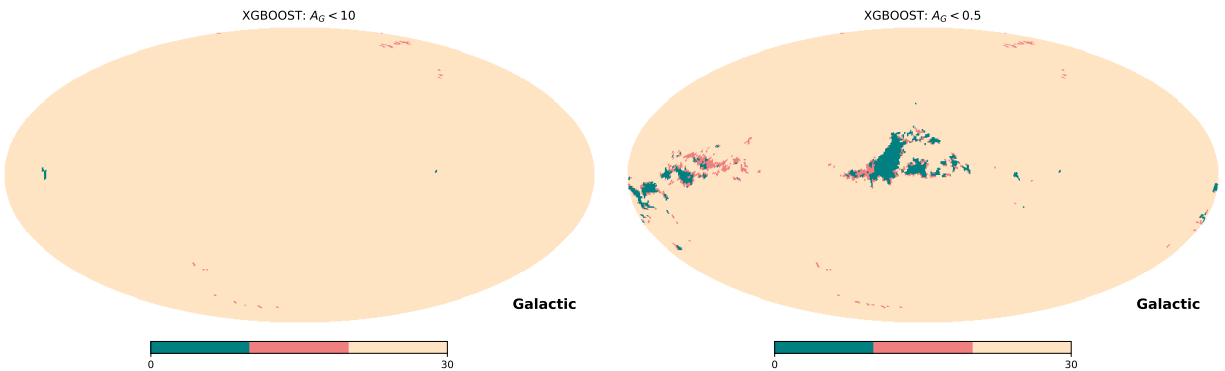


Figure 2: Number density of candidate guide stars (per 0.32 square degree) from the xgboost catalog with apparent magnitude $10 < G < 17$. Most of the sky has enough stars for guiding the Roman, except for a few small patches.

2.4 Number density of candidate guide stars on the sky for various catalogs

For guiding, we need a minimum of 4 and a maximum 18 guide stars with at most one star per detector. In what follows, we adopt the bounding box of the WFI, which has an area of 0.32 square degree, as our fiducial area for working with the number density of guide stars. The active light sensitive area of WFI is 0.28 square degrees. Hence, 18 stars over the light sensitive area of WFI is equivalent to 20 stars over 0.32 square degree and we adopt this as our desired threshold for number density. A density smaller than this threshold increases the risk of failing to get the minimum number of good quality guide stars for a number of reasons. First, due to Poisson noise, even if we adopt 20 stars on average, a given WFI sized regions can have less than 4 stars, and the probability of this happening increases if we lower the threshold. Secondly, out of the selected stars some stars may have peculiar properties making them unsuitable to be used as guide stars. Finally, the requirement of 1 star per detector also means stars should not be clustered. In general, choosing guide stars that are as far apart as possible helps to improve the precision of guiding.

For guiding we prefer stars that are bright (to have high signal to noise ratio) and have reliable spectroscopic parameters (based on the new approach outlined in [subsection 2.2](#)). We investigated how different spectroscopic parameter selection criteria for various catalogs restricted the number of bright stars available as candidate guide stars. For this, we computed the number density for each case in healpix patches of $N_{\text{side}} = 64$ (area of about 0.84 square degrees that is of the order of the WFI area). Ideally, it would have been desirable to use healpix with a larger N_{side} (smaller patch area), to make sure every detector sized region of sky has enough guide stars. However, a smaller area will lead to higher variance in the estimated number density. A lower healpix order would give robust density estimate but the patch area would be too large to be representative of the WFI field of view. The number density results are summarized in [Table 1](#). We begin by investigating if there are enough bright stars in the 2MASS catalog. A color cut of $-0.5 < (J - K_s) < 1.05$ was applied to get rid of stars that are too hot or too cold. Results show that we have enough stars in the range $10 < K_s < 13$, but might have to go to K_s of 14 in some areas. The RVS spectrograph of *Gaia* provides good spectroscopic stellar parameters for about 5.5 million stars with brightness roughly upto $G \sim 12.5$. However, 36% of the sky has number density that is below our threshold for stars with RVS observations. The `xgboost` catalog based on BP/RP spectra consists of 172 million stars and extends to about $G \sim 17.65$. Hence, in principle it should have enough stars and this is confirmed in [Table 1](#). However, there is a minor fraction of the sky (0.096% or 39 square degrees) that have a number density below our threshold of 20 ([Figure 2](#)). Two patches with total area of about 11 square degrees (0.026% of sky) have number density close to zero, they lie close to the Galactic plane with (l, b) of $(155, 0)$ and $(83, 0)$. The exact cause of this is not known but it is most likely related to issues with either the quality or processing of *Gaia* (or `xgboost` catalog) data in this region. Later on in [subsection 3.1.1](#), we show that it is difficult to estimate the Roman magnitude of a star that has high extinction. Hence, we also estimated the missing sky fraction of stars in the `xgboost` catalog that have low extinction and found that even if we restrict to stars with low extinction we have enough stars over most of the sky for guiding purposes.

2.5 Estimating the apparent magnitude in Roman pass bands

In the proposed model, [Equation 5](#) predicts the apparent magnitude of a star in a desired band given its stellar properties like apparent magnitudes, metallicity and extinction. Technically, this is

Table 2: Base regression schemes/models

Scheme	Input variables		
	$B1$	$B2$	other variables
A	G_{RP}	G_{BP}	$(A_G, [M/H])$
B	G_{RP}	G_{BP}	
C	K_s	J	
D	G		
E	G_{RP}	G_{BP}	$[M/H]$

a case of statistical regression for estimating a dependent variable Y given a set of feature vectors (independent variables) X . Given a training set consisting of Y and X values for a large number of stars this can be easily accomplished. When we have the parallax information ω available, we estimate the parameter f_{giant} and use [Equation 6](#) to estimate the apparent magnitude. This requires the use of both the giant and the dwarf models to estimate the final answer.

The independent variables that we are interested in are the *Gaia* magnitudes (G, G_{BP}, G_{RP}), 2MASS magnitudes (J, K_s), the extinction A_G from *Gaia* gspphot and stellar parameters $[M/H], T_{\text{eff}}$ and $\log g$ from the *xgboost* pipeline. The `numpy.linalg.lstsq` was used to determine the model parameters (polynomial coefficients), with $Y = y - m_{B1}$ and $X = [x, x^2, x^3, x^4, [M/H], A_G, A_G^2, A_G x]$, where $x = m_{B2} - m_{B1}$ is the color and m_{B1} and m_{B2} are the magnitudes in two chosen photometric bands.

Depending on the choice of the input variables and training sets one can construct various different models. We derived results for four different models (A, B, C, D and E) categorized based on choice of input X ([Table 2](#)). For each base class of models, we derived model parameters for three different training sets, i) having giant stars ii) having dwarf stars and iii) having stars of all types; with the star class variable l of [subsection 2.2](#) for them being giant, dwarf and none respectively. Stars in the training set were classified as either dwarf or giant using [Equation 2](#). The fitting parameters are given in [subsection 5.3](#) (see [Table 7](#), [Table 8](#), [Table 9](#), [Table 10](#) and [Table 11](#)). When ω is used ([Equation 6](#)) we denote the scheme by adding subscript 1 and when it is not used ([Equation 5](#)) we use subscript 0, e.g., schemes A_1 and A_0 .

2.5.1 The training set

For our training set we use *Gaia* stars with spectroscopic stellar parameters estimated from *Gaia* RVS spectra, good quality 2MASS photometry, valid value for extinction, and valid values for XP spectroscopic stellar parameters (from *xgboost*).

$$\begin{aligned}
 & (1000 < T_{\text{eff,gspspec}} < 20000) \ \& \ (t\text{mass_ph_qual} = \text{AAA}) \ \& \\
 & (A_G \neq \text{null}) \ \& \ (G \neq \text{null}) \ \& \ (G_{BP} \neq \text{null}) \ \& \ (G_{RP} \neq \text{null}) \ \& \\
 & (T_{\text{eff,xgboost}} \neq \text{null}) \ \& \ (\log g_{\text{xgboost}} \neq \text{null}) \ \& \ ([M/H]_{\text{xgboost}} \neq \text{null})
 \end{aligned} \tag{7}$$

For computational ease, we take a random subsample of these stars (1/10-th of the sample obtained by filtering based on the last digit of the healpix level 6 index being 1). This results in about 290,000 stars. We supplement additional columns like XP spectra based stellar parameters from ([Andrae et al. 2023a](#)).

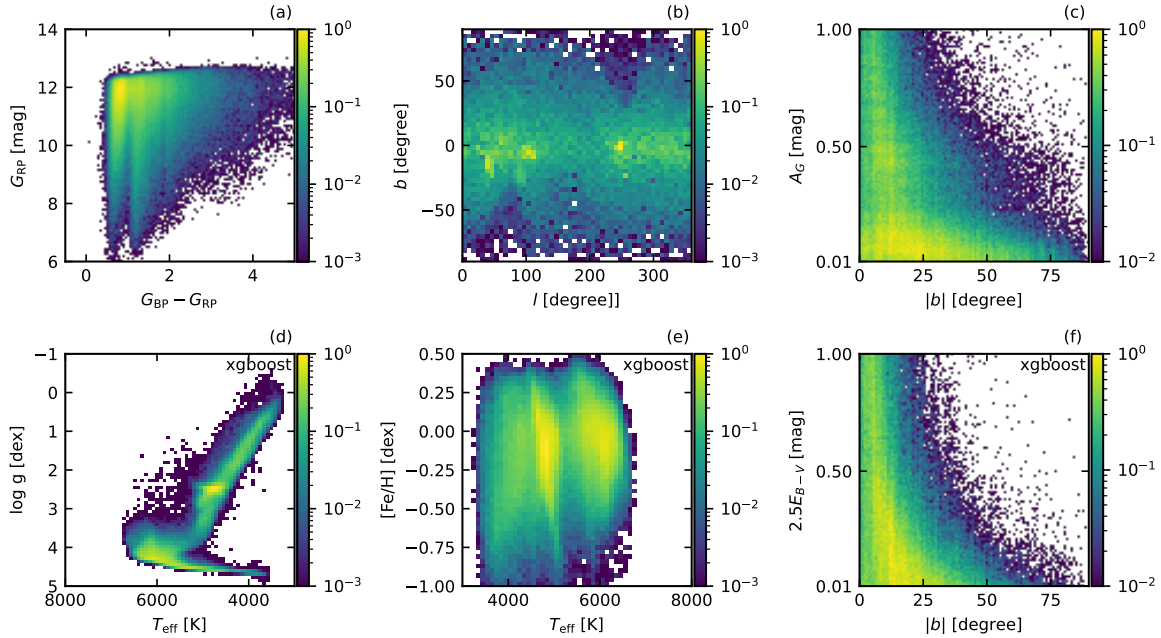


Figure 3: Overview of the training set used to derive apparent magnitude relations. Shown are the distributions of: *Gaia* G_{BP} , G_{RP} magnitudes; Galactic coordinates l , b ; *Gaia* DR3 extinction A_G ; and XP spectra based estimates of T_{eff} , $\log g$ and $[M/H]$, E_{B-V} (Andrae et al. 2023a, XGBOOST). In each panel the probability density is normalized to have a maximum value of 1.

Only about 88% of *Gaia* *xgboost* stars have a valid measurement of A_G in *Gaia* DR3. We could have estimated A_G using *xgboost* stellar parameters and used that in Equation 5. However, there was more uncertainty in the predictions of the regression model when using $A_{G,\text{xgboost}}$ as compared to $A_{G,\text{gspphot}}$ (RMS for *Gaia* G band of 0.016 dex as compared to 0.012 dex). Additionally, stars with invalid values of $A_{G,\text{gspphot}}$ also showed more uncertainty as compared to stars with valid values (uncertainty for *Gaia* G band of 0.023 dex as compared to 0.016 dex). Hence we adopt the *Gaia* DR3 A_G .

An overview of the properties of the training set is given in Figure 3. Panel-a shows that stars belong to a wide range of colors and apparent magnitudes. Panel-b (top middle) shows that stars are distributed all over the sky spanning both low and high Galactic latitudes. Panel-c (top right) shows extinction as a function of Galactic latitude $|b|$. The extinction A_G is high in the Galactic plane and decreases with increase of Galactic latitude $|b|$. Panel-f (bottom right) shows extinction as estimated by comparing observed color with those estimated using the *xgboost* stellar parameters and the synthetic spectra, and is in good agreement with *Gaia* A_G values. Panels-(d,e) show the distribution of spectroscopic stellar parameters from the *xgboost* catalog, again confirming that we have stars with a wide variety of temperature, gravity and metallicity.

Color magnitude diagram of stars in the training set for high and low Galactic latitude regions is shown in Figure 4. Stars in the low latitude regions are significantly affected by dust. An evidence of this is that at low latitudes (right panel) the red clump, which is normally around $(G_{BP} - G_{RP}, M_G) \sim (1.25, 0)$ as seen in the left panel, is spread out diagonally along the direction of the extinction vector in the right panel. The dashed line shows the equation used to separate giant

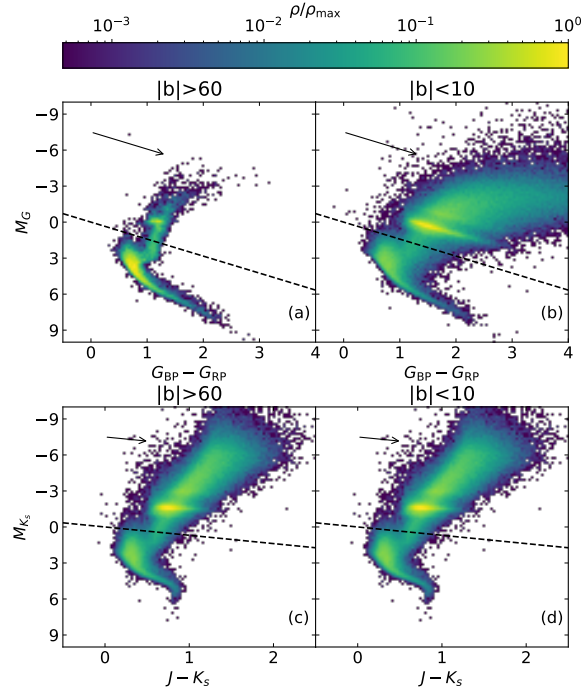


Figure 4: Color magnitude diagram of stars in the training set for high (left column) and low (right column) Galactic latitude regions. The arrow shows the extinction vector and the dashed line shows the line (Equation 2) used to separate giants from dwarfs

from dwarfs, which is intentionally designed along the extinction vector so that the classification remains unaffected by extinction.

2.5.2 Estimating apparent magnitudes of stars in the training set from stellar spectra library

The training set provides stellar parameters ($T_{\text{eff}}, \log g, [M/H]$) and apparent magnitude in *Gaia* passbands. We now discuss the method to estimate the apparent magnitude in any other passband using information available in the training set. The apparent magnitude m_λ depends on absolute magnitude M_λ , the distance modulus μ and extinction E_{B-V} by

$$m_\lambda = M_\lambda + \mu + E_{B-V}R_\lambda. \quad (8)$$

The pseudo absolute magnitude $M'_\lambda = M_\lambda + c$, which is absolute magnitude up to a constant, can be estimated if we know the spectrum of a star and the throughput curves of the passband we are interested in. We create new variable $\mu' = \mu - c$ to absorb the constant c in it leading to

$$m_\lambda = M'_\lambda + \mu' + E_{B-V}R_\lambda. \quad (9)$$

The spectrum of a star can be estimated from stellar parameters ($T_{\text{eff}}, \log g, [M/H]$) by using spectral libraries. The extinction coefficient R_λ is in general a function of stellar parameters

Table 3: The zero point of Roman passbands. The listed coefficients are for use in Equation 13 in Reinhart (2023) and it replaces Table 9 of that report.

Roman band	WFI Detector	Z_R	σ_Z	$\alpha_{\min,R}$	A_λ/E_{B-V}
f062	1-18	26.6179	0.0415	200	2.6048
f087	1-18	26.3023	0.0291	200	1.5902
f106	1-18	26.3546	0.0338	200	1.1495
f129	1-18	26.3531	0.0382	200	0.8497
f146	1-18	27.5842	0.0339	200	0.8030
f158	1-18	26.3760	0.0330	200	0.6140
f184	1-18	25.9124	0.0334	200	0.4794
f213	1-18	25.8633	0.0385	200	0.3804
prism	1-18	27.6512	0.0263	50	0.9899
grism	1-18	26.9882	0.0376	50	0.7720
prism.b8	1-18	23.9919	0.0276	50	1.4465
prism.r8	1-18	24.3673	0.0352	50	0.8298
grism.b8	1-18	22.1296	0.0382	50	1.1324
grism.r8	1-18	21.4872	0.0370	50	0.4688

($T_{\text{eff}}, \log g$). The use of R_λ is a convenient way to handle the effect of extinction which in reality requires integrating over the spectral energy distribution. Next, we solve for the two unknowns μ' and E_{B-V} in Equation 9, by making use of observed apparent magnitudes and estimated pseudo magnitudes in the *Gaia* BP and RP bands. We now have everything to estimate the apparent magnitude in any given passband. Note, for broad pass bands like that of *Gaia*, the extinction coefficient R_λ varies with both T_{eff} and $\log g$. To take this into account, we use R_λ estimated from Padova isochrones Marigo et al. (2017). For Roman pass bands we assume R_λ to be independent of T_{eff} and $\log g$ as the bands are narrow and the variation is expected to be small. More specifically, R_λ was estimated for a spectrum with solar parameters, ($[M/H], T_{\text{eff}}, \log g$) = (0.0, 5770K, 4.438), by determining the change in apparent magnitude for a change in E_{B-V} of 1. Finally, to estimate the count rates it is necessary to know the zero points and they are related to count rate α_R by

$$Z_R = m_R + 2.5 \log_{10} \frac{\alpha_R}{e^{-s^{-1}}} \quad (10)$$

We make use of the above equation to compute the zeros points for the Roman passbands by taking a constant flux spectrum and applying the throughput curves to it. The zero points and extinction coefficients for different Roman bands are listed in Table 3. Although we assume a single zero point for all detectors, in reality the zero points are not same as the throughput curves vary from detector to detector. The zero point variation is described by σ_Z , which is the standard deviation in zero point among the 18 detectors.

We use the Phoenix synthetic stellar spectra library (Allard et al. 2012) to estimate the absolute magnitudes in Roman bandpasses. Phoenix stellar spectra library was chosen for its improved spectral coverage over the range of stellar parameters and its completeness of spectral features compared to the previously used Pickles data. For a given star, we start with `xgboost` based stellar parameters ($T_{\text{eff}}, \log g, [M/H]$) and estimate the spectrum corresponding to those parameters, using the `stsynphot.grid_to_spec` function which interpolates between stellar parameters over the grid of stellar templates to predict individual stellar spectra. Model photometry was then calculated from the interpolated model stellar spectra using `synphot`. Note, the phoenix library provides stellar spectra for a given ($T_{\text{eff}}, \log g, [M/H]$), but the flux of the spectra is unnormalized

Table 4: AB to Vega magnitude conversion factors for Gaia and 2MASS passbands.

band	$\Delta_{\text{AB-Vega}}$	Z_{offset}
2MASS J	0.91338	0.046
2MASS H	1.39118	0.0
2MASS K_s	1.86344	0.032
<i>Gaia</i> G	0.127432	-0.033
<i>Gaia</i> G_{BP}	0.02385	-0.047
<i>Gaia</i> G_{RP}	0.02385	-0.022

as the total luminosity (or radius) is unspecified. Hence, we use the *Gaia* G_{RP} band as the base band and normalize the spectrum to have $G_{\text{RP}} = 0$. Interpolating over individual spectra is slow, hence we pre-computed AB magnitudes in all desired bandpasses (Roman and as well as Gaia and 2MASS that are in the GSC) over a regular grid in $([M/H], T_{\text{eff}}, \log g)$ space spanning the extent covered by the GSC. Interpolation is then used to compute values for any given stellar parameter using `scipy.interpolate.RegularGridInterpolator`. See [subsection 5.2](#) for a comparison of results from interpolated photometry to one computed from interpolated spectra.

To estimate photometry from a spectrum, `synphot` requires the specification of passbands. Passbands for *Gaia*, Roman and 2MASS were constructed from throughput curves. For Roman the latest throughput curves were used ⁵. The throughput curves vary across the 18 detectors, but we used the average throughput as the differences are small (less than 0.05 mag, see σ_Z in [Table 3](#)) compared to our required precision (about 1 mag, see [subsection 3.1.1](#) for further discussion). The estimated synthetic magnitudes are in AB system, while the cataloged photometry of *Gaia*, 2MASS and WISE are in the Vega system. Thus for these bands we convert the estimated AB magnitudes to Vega magnitudes using

$$m_{\text{Vega}} = m_{\text{AB}} - (\Delta_{\text{AB-Vega}} + z_{\text{offset}}), \quad (11)$$

where $\Delta_{\text{AB-Vega}}$ is a conversion factor estimated using the python `synphot` package, and z_{offset} is a small offset which was applied to minimize the difference between the synthetic and observed photometry of stars in the training set. The adopted values of $\Delta_{\text{AB-Vega}}$ and z_{offset} are listed in [Table 4](#).

2.5.3 Estimating apparent magnitudes and count rates for dispersive elements of WFI

The WFI also has two dispersive elements, a grism and a prism, which will also be used for guiding during observations. The dispersive elements leave an elongated trace on the detector, with well defined sharp edges, which will be used for guiding. An essential step in guiding is to locate either a center (for spherical shapes) or an edge (for elongated shapes) of a target image on the detector. Due to the steepness of the edges, locating an edge works well in simulations with well separated stars. However during real observations there is a high likelihood for confusion due to traces from many neighboring stars.

To confirm that the correct guide star has been selected, a flux check needs to be done. The guide star acquisition process involves two steps (for details see [Reinhart 2022](#)) and an independent flux check is done for each of them. In the first step, the long side of the 170x24 pixel guide

⁵<https://github.com/spacetelescope/roman-technical-information>

window is placed close to the middle of the guide star spectrum and perpendicular to the dispersion direction. The flux from any spectral component detected in the guide window is compared to pre-computed expected typical value for the desired guide star. This typical value is determined from the total flux through the entire dispersive element, which we compute by treating the throughput curve of the entire dispersive element as a passband.

In the second step, the long side of the guide window is placed parallel to the observed spectrum. Next, centering is done by aligning the edge of a template spectrum to that of the observed spectrum and this is followed by a flux check. Pixels within an eight-pixel long region of the spectrum closest to bright end of the guide window are summed along the axis perpendicular to the dispersion direction. The 8 flux values are then averaged to estimate the edge flux for that particular guide star. For the current guide window sizes (128x32) this results in the averaging of the pixels 56-64 from the edge of the spectrum. The edge of the spectrum is defined as the two wavelengths where the throughput is equal to half the typical value (defined as the average region with throughput greater than 0.01) of the dispersive region. The edge flux is compared to a pre-computed expected value which we aim to provide in this report. We compute the edge fluxes by treating the 8 pixel wide regions of the spectrum as photometric bandpasses, the photometry are referenced by the `_b8` and `_r8` suffixes on the `prism` and `grism` labels for the blue and red edge respectively. Note, the photometric values are calculated based on the sum of the eight-pixel region and thus the predicted count rates need to be normalized by 8 before they are compared with the observed edge flux count rates.

3 RESULTS AND DISCUSSION

3.1 Different regression models based on the choice of base magnitudes and stellar parameters

In general, with more stellar parameters and better precision, our ability to estimate the apparent magnitudes in the Roman bands improves. Hence, for selecting guide stars, where accuracy of estimates is important, it makes sense to use a large set of stellar parameters. In our tests we found that using the following five parameters ($G_{BP}, G_{RP}, A_G, [M/H], \omega$) gives good estimates of magnitudes in the Roman bands (scheme A_1). However, not all of the above parameters will be available for all stars, especially the faint stars which are likely to act as spoilers if they are close to a guide star. Hence it is necessary to devise multiple methods to estimate magnitudes in the Roman bands. Below we describe four schemes for estimating magnitudes in the Roman bands, for summary see [Table 2](#). They are ranked in increasing order of uncertainty in the estimated magnitudes. For each of them we could choose to either use the parallax or ignore it (see [Equation 6](#) and [Equation 3](#)).

- Scheme A: Estimates using ($G_{BP}, G_{RP}, A_G, [M/H]$): This is the set that gives lowest uncertainty in estimated Roman magnitudes. It is suitable for selecting guide stars.
- Scheme B: Estimates using (G_{BP}, G_{RP}): For a significant number of stars several of the stellar parameters described in method A are not available. Out of 1.56 billion stars having G_{BP} and G_{RP} , extinction A_G is available for only 470 million stars. The $[M/H]$ is only available for some 175 million stars as it comes from publicly available BP-RP spectra which

is only available for some 219 million stars with $G < 17.6$. This method is suitable for selecting guide stars when A_G or $[M/H]$ are not available.

- Scheme C: Estimates using (J, K_s) : Although 2MASS, which is an all-sky near-infrared survey, is in general shallower than *Gaia*, it may detect some faint red stars which *Gaia* fails to detect. As Roman is primarily a near-infrared survey it is important to detect faint red stars. Hence we devise a method to estimate the Roman magnitudes from just the 2MASS magnitudes (J, K_s) . The reason *Gaia* might miss some 2MASS stars is due to the fact that *Gaia* observes in the visual band whereas 2MASS observes in near-infrared. Hence, red stars are fainter in *Gaia*. Additionally, extinction being stronger for visual bands, in regions with high extinction, some stars might be too faint to be detectable in *Gaia* but might be detectable in near-infrared and infrared bands. This method is suitable for selecting guide stars but may be more relevant for selecting faint, red spoiler stars.
- Scheme D: Estimates using only G : About 300 million very faint stars in *Gaia* only have G band magnitudes and no other stellar parameters, this method is for those stars. This method is suitable for selecting spoiler stars only.
- Scheme E: Estimates using $(G_{BP}, G_{RP}, [M/H])$: This is an extra scheme that was constructed just to individually test the effect of $[M/H]$ and A_G on the accuracy of predicted magnitudes. This method is not intended to be used for selecting either guide stars or spoiler stars.

3.1.1 Comparison of the accuracy of the different regression models

The primary purpose of predicting apparent magnitudes (or count rates) is to compare these values against observations, thereby validating the identification of guide stars. While there is no formal requirement for the accuracy of the predictive relations, the precision of these derived relations inherently sets the lower bound on the tolerance (i.e., the allowed difference) used for guide star selection. Currently, the adopted tolerance between observed and predicted magnitudes is ± 2 magnitudes, which is relatively broad. Ideally the tolerance should vary with the stellar number density. In sparse fields, a larger tolerance may be acceptable; however, in crowded regions, a more stringent tolerance is necessary to minimize the risk of incorrect guide star acquisition (misidentification). With this motivation in mind, we now discuss the accuracy of our regression models.

A comparison of the accuracy of the different regression models is shown in [Figure 5](#). Residuals of the predicted 2MASS K_s magnitude as compared to the actual observed values is shown as a function color $G_{BP} - G_{RP}$, absolute magnitude $M_{G_{RP}}$ and extinction A_G for various regression models. Each row shows results of one regression model. We start with just the apparent magnitudes G_{BP} and G_{RP} (regression scheme B_0). Going from top to bottom, progressively more parameters like $[M/H]$, A_G and ω are added, namely schemes E_0 , A_0 and A_1 . The root-mean-square (RMS) and median-absolute-deviation (MAD) of the residuals are labeled on each panel; for the training set restricted to color $G_{BP} - G_{RP} < 2$ (left panels), for the full training set (middle panels), and for the training set restricted to $A_G < 0.5$ (right panels). The plotted data points in each row are the same. Note, the dependent variable in the regression is the observed 2MASS K_s magnitude, so in these plots there is no use of synthetic spectra. In [Figure 6](#), we repeat the same

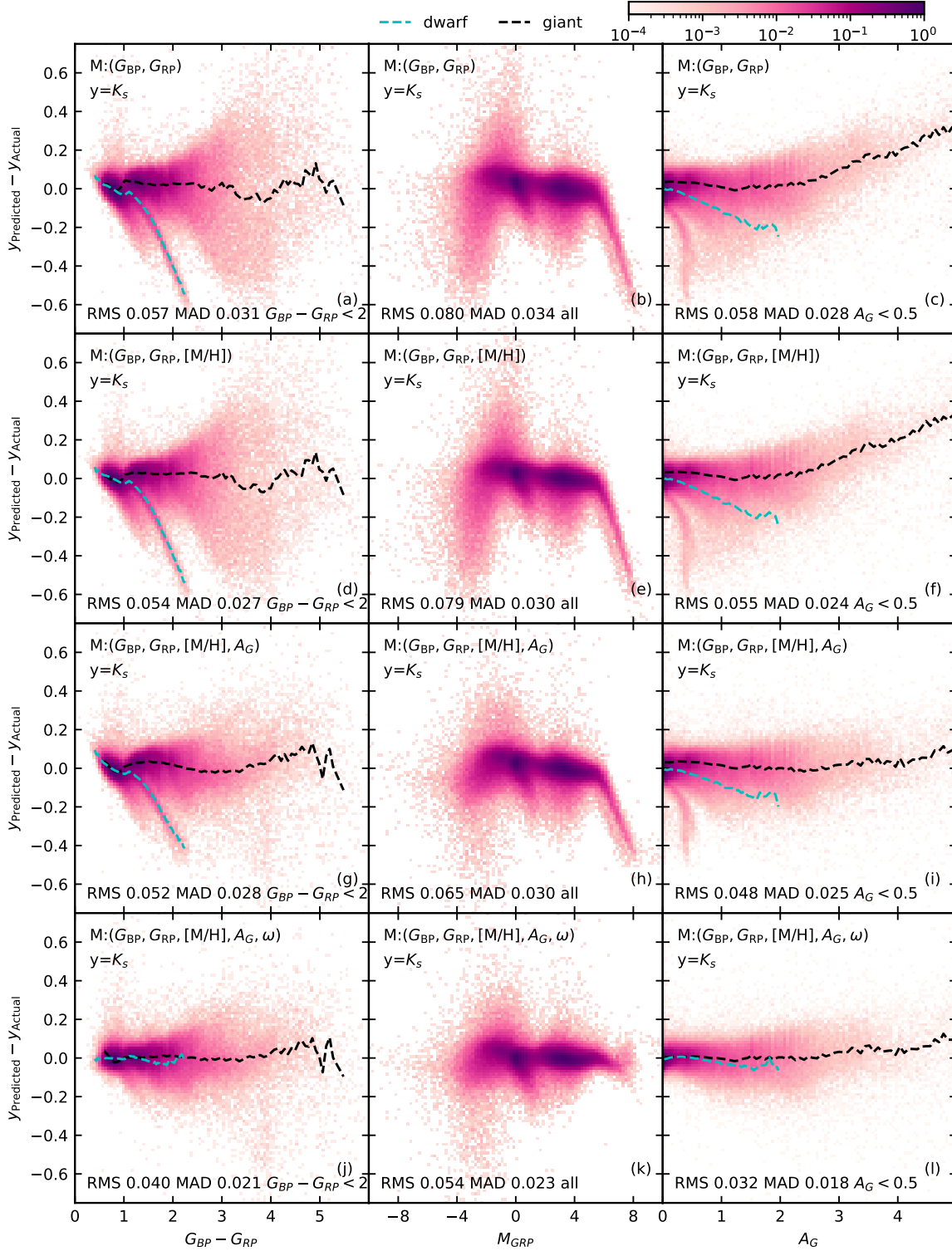


Figure 5: Residuals of 2MASS K_s magnitude predicted by various regression models as compared to the actual values. Residuals are shown as a function of color $G_{BP} - G_{RP}$, absolute magnitude M_{GRP} and extinction A_G . The features used in the regression model are labeled on each panel. Each row corresponds to results from one given model. From top to bottom the models are in the following order (B_0 , E_0 , A_0 , A_1). Density is normalized to have a maximum density of 1.

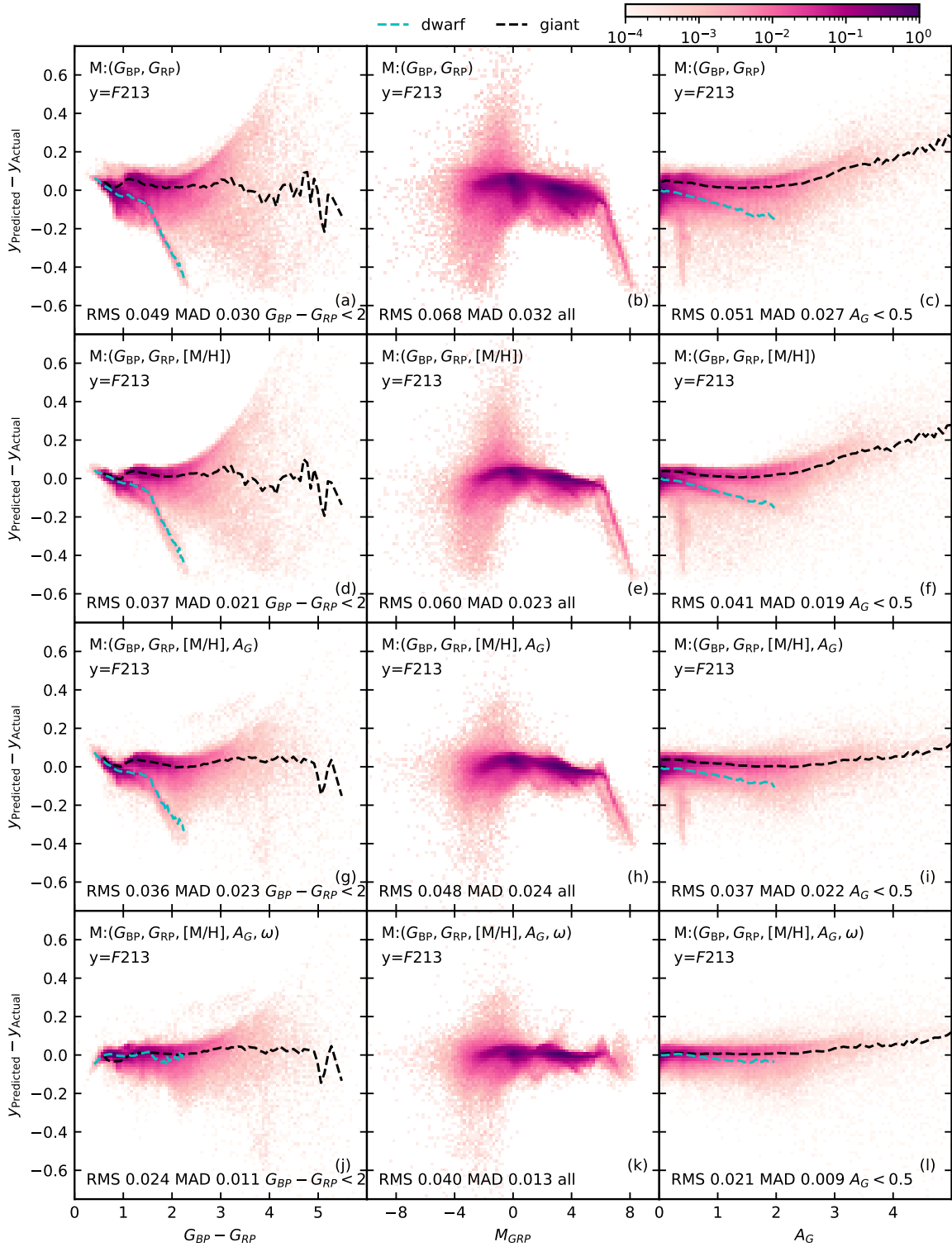


Figure 6: Residuals of Roman $F213$ magnitude predicted by various regression models as compared to the actual values. Residuals are show as a function of color $G_{BP} - G_{RP}$, absolute magnitude M_{GRP} and extinction A_G . Each row corresponds to results from one given model. From top to bottom the models being (B_0, E_0, A_0, A_1) . Density is normalized to have maximum density of 1.

analysis as done in [Figure 5](#) but for the Roman $F213$ band instead of the 2MASS K_s band, and those plots make use of our synthetic spectra. We chose $F213$ as its central wavelength is close to that of K_s . Overall the trends and features seen in [Figure 6](#) are very similar to that in [Figure 5](#). This is reassuring, as it validates the pipeline of synthetic photometry that we use to predict the magnitudes in Roman bands.

The RMS and MAD values, which track the accuracy, decrease consistently from top to bottom with the addition of each extra parameter to the regression model. The fact that introduction of $[M/H]$ leads to smaller spread in residuals can be seen by comparing panel-b with panel-e of [Figure 6](#) at $M_{GRP} \sim 4$. Comparison of panel-f with panel-i in both [Figure 5](#) and [Figure 6](#) clearly shows that introducing A_G gets rid of the systematic trend with A_G seen in panel-f.

The dashed lines show the mean residual profiles for the giant and dwarf sub-samples. The dwarfs with $G_{BP} - G_{RP} > 1.5$ and $M_{GRP} > 5$ show large systematic errors of up to 0.4 mags, visible as long narrow streaks in the panels in the top three rows of both [Figure 5](#) and [Figure 6](#). These systematic errors vanish when parallax, ω , is used as a model parameter (bottom row). The panels in the bottom rows show that even for our best model, the error increases with A_G , and consequently the RMS error is about 40% smaller if restricted to $A_G < 0.5$. A reduction in error is also achieved by restricting to stars with $G_{BP} - G_{RP} < 2$, as it eliminates the highly extinguished red stars, but it is not as effective as restricting stars by A_G .

In addition to the trends matching and being more pronounced for $F213$ in [Figure 6](#), the overall RMS values are about 30% smaller. This is because the 2MASS K_s values are real measurements with measurement uncertainties of about 0.02 mags, which will add up in quadrature to the intrinsic scatter of the K_s residuals. On the contrary, the $F213$ values are synthetic estimates with zero uncertainty and hence their residuals are expected to have smaller scatter as compared to that of the K_s . Assuming that $F213$ residuals are a measure of the intrinsic RMS error of the regression based estimates, we see that the intrinsic scatter is comparable to that of the 2MASS photometric uncertainties (0.02 dex) if restricted to low extinction but in general it could be a factor of two higher (0.04 dex).

RMS uncertainty for all Roman bands for each of the schemes both with and without ω is shown in [Table 5](#). It confirms that the trends we found for $F213$ in [Figure 6](#) are also valid for other bands: namely the more the parameters in the model, the lower the errors; this can be seen by comparing errors in columns 2, 3, 5 and 7 for any given row. When using the G_{BP} (532 nm) and G_{RP} (797 nm) bands of *Gaia* as input (schemes A and B), the error is found to systematically increase with increase in effective wavelength of a band (going from passband $F062$ to passband $F213$). The only exception is passband $F146$, which being significantly wider than the other bands behaves slightly differently. Scheme C, which uses 2MASS bands J (1250 nm) and K_s (2150 nm) as input, shows a different trend—with increase of effective wavelength the error first decreases, till $F106$, and then increases. This suggests that for a given output band lowest error is obtained by choosing an input band closest to the output band, which intuitively makes sense. However, the general conclusion that error increases with effective wavelength also seems to be true for scheme C—the error of $F213$ is still higher than $F129$, despite the output band being close to one of the input bands in both cases. The MAD uncertainty is shown in [Table 6](#), it is about a factor of 3 less than the RMS uncertainty, as compared to 1.5 expected for a normal distribution, suggesting that the majority of stars have uncertainty that is less than the RMS value. This discrepancy arises because the residual distribution is leptokurtic (long tailed) and contains significant outliers. Therefore, we recommend using the RMS to define the selection tolerance for selecting guide stars. Unlike

Table 5: Root mean square uncertainty in estimating the apparent magnitude in the Roman band-passes from columns in the GSC catalog. Results for various methods both with and without the use of parallax are shown.

band	A ($G_{BP}, G_{RP}, A_G, [M/H]$)		B (G_{BP}, G_{RP})		C (J, K_s)		D (G)	
	With ω ?		With ω ?		With ω ?		With ω ?	
	yes (A_1)	no (A_0)	yes (B_1)	no (B_0)	yes (C_1)	no (C_0)	yes (D_1)	no (D_0)
f062	0.008	0.009	0.010	0.011	0.156	0.158	0.131	0.191
f087	0.014	0.014	0.019	0.019	0.059	0.059	0.373	0.507
f106	0.024	0.026	0.035	0.036	0.039	0.040	0.467	0.640
f129	0.031	0.035	0.044	0.048	0.043	0.044	0.539	0.753
f146	0.028	0.033	0.041	0.047	0.045	0.046	0.563	0.789
f158	0.035	0.043	0.052	0.060	0.054	0.055	0.615	0.877
f184	0.040	0.049	0.058	0.068	0.061	0.064	0.658	0.941
f213	0.040	0.048	0.058	0.068	0.068	0.070	0.674	0.960
prism	0.024	0.027	0.035	0.038	0.040	0.041	0.516	0.717
grism	0.030	0.035	0.043	0.049	0.046	0.047	0.569	0.800
prism_b8	0.018	0.018	0.024	0.024	0.049	0.050	0.403	0.547
prism_r8	0.032	0.035	0.044	0.048	0.043	0.044	0.544	0.761
grism_b8	0.028	0.030	0.038	0.040	0.041	0.041	0.470	0.650
grism_r8	0.037	0.047	0.056	0.068	0.062	0.064	0.658	0.941

the robust MAD, the RMS accounts for the observed outliers and distribution tails, ensuring the probability of large residuals is not underestimated when setting selection limits.

3.1.2 Under what circumstances is it worth using the parallax information?

Using parallax, ω , increases precision but adds complexity to our regression scheme. The usefulness of using parallax depends upon the scheme used and its intended use. If the intended use is to select guide stars one should try to get the best estimate of apparent magnitude, and hence one should use the parallax information. However, when we just want to screen the spoilers, we can sacrifice some accuracy and compute the apparent magnitude without the use of parallax. In [Table 5](#) focusing on the red band F213, we see that among schemes A,B and C; scheme A has the largest percentage decrease in RMS error when using parallax, followed by scheme B and then scheme C. For scheme *B* the gain in precision by including parallax is modest while for *C* it is negligible. For scheme *D* it might seem that there is a significant gain by including parallax, but the stars for which this scheme would be used would be very faint $G > 20$ and they will have high parallax uncertainty, which will erode any benefit of using parallax. The above discussion suggests that it is prudent to use parallax with scheme A, but one can ignore parallax when using schemes B,C and D. Finally, when using parallax, we take the logarithm (see [Equation 4](#)), this demands that parallax be positive. Given that uncertain parallax is not too useful either, one could restrict to using parallax when the ratio $\omega/\sigma_\omega > 3$, where σ_ω is uncertainty in measurement of parallax.

Based on the discussion above we propose to use scheme A_1 (with parallax) for the actual guide stars. Coefficients for these are given in [Table 7](#) and [Table 8](#). For stars for which scheme A_1 cannot be applied, we propose to use schemes B_0 , C_0 or D_0 (ranked in decreasing order of priority) all of which do not use parallax, coefficients for these are given [Table 9](#), [Table 10](#) and [Table 11](#). The precision of this scheme should be sufficient to identify spoilers around guide stars. Finally

Table 6: Median absolute deviation (MAD) uncertainty in estimating the apparent magnitude in the Roman bandpasses from columns in the GSC catalog. Results for various methods both with and without the use of parallax are shown.

band	A ($G_{BP}, G_{RP}, A_G, [M/H]$)		B (G_{BP}, G_{RP})		C (J, K_s)		D (G)	
	With ω ?		With ω ?		With ω ?		With ω ?	
	yes (A_1)	no (A_0)	yes (B_1)	no (B_0)	yes (C_1)	no (C_0)	yes (D_1)	no (D_0)
f062	0.002	0.003	0.004	0.004	0.073	0.073	0.075	0.132
f087	0.005	0.006	0.009	0.009	0.033	0.033	0.181	0.328
f106	0.009	0.012	0.016	0.017	0.022	0.022	0.225	0.416
f129	0.010	0.016	0.016	0.020	0.019	0.020	0.265	0.497
f146	0.010	0.017	0.015	0.021	0.019	0.020	0.276	0.522
f158	0.012	0.021	0.020	0.029	0.021	0.024	0.309	0.589
f184	0.014	0.024	0.024	0.034	0.023	0.026	0.331	0.634
f213	0.013	0.024	0.021	0.032	0.024	0.028	0.337	0.643
prism	0.008	0.013	0.014	0.017	0.020	0.020	0.251	0.470
grism	0.010	0.018	0.015	0.022	0.019	0.021	0.281	0.530
prism_b8	0.007	0.008	0.011	0.011	0.028	0.028	0.196	0.354
prism_r8	0.009	0.016	0.015	0.019	0.019	0.020	0.269	0.504
grism_b8	0.010	0.014	0.016	0.018	0.021	0.022	0.228	0.425
grism_r8	0.012	0.025	0.021	0.033	0.023	0.026	0.330	0.631

for determining T_{eff} , as required by spectroscopic guiding, we propose to use the T_{eff} value from the `external.xgboost` catalog—being based on the XP spectra, this T_{eff} will be much more accurate than one derived purely from photometric colors.

4 SUMMARY AND CONCLUSIONS

The primary objective of this technical report was to develop precise analytical models to predict the apparent magnitude and count rates of stars in the Roman Wide-Field Instrument (WFI) pass bands based on the information that is readily available, for example the columns available in the GCS catalog. The Roman telescope will utilize the WFI for guiding, necessitating an accurate estimation of stellar flux for both guide stars and their neighbors. Building upon the formalism of [Reinhart \(2023\)](#), our study developed a more sophisticated approach by incorporating, in addition to *Gaia* apparent magnitudes, stellar parameters—namely, parallax, extinction and metallicity—into the predictive model. We used a multivariate polynomial to express the Roman magnitude as a function of these variables, which were sourced from updated catalogs like *Gaia* DR3 and the external *Gaia* `xgboost` catalog (which is now available in the GSC). Some of our main findings are as follows.

The use of parallax, extinction and metallicity all improve the ability of regression models to predict the apparent magnitude. However, not all stars will have measurements of the required stellar properties. Hence, we propose four different models, A_1 , B_0 , C_0 and D_0 (in decreasing order of accuracy) that can cater to a wide variety of situations. Most precise estimates are obtained with model A_1 which uses the following five stellar properties ($G_{BP}, G_{RP}, A_G, [M/H], \omega$). The model predictions have an RMS uncertainty of 0.01 mag for the bluer bands and 0.04 mag for the redder bands, while the MAD uncertainty is at least a factor of 3 lower. We propose this to be used for

selecting guide stars, where high accuracy is needed. Even for our best model, the uncertainty was found to increase with extinction. Hence we recommend restricting to stars with low extinction.

The other simpler models like B_0 , C_0 and D_0 should be useful for detecting spoiler stars, where one can work with reduced accuracy. The model B_0 , which makes use of only (G_{BP}, G_{RP}) has an RMS uncertainty of 0.068 mag, which is only slightly higher than A_0 . However, we show that in such models for certain specific types of stars (red dwarfs and stars with high extinction) there are systematic errors of upto 0.6 dex. Hence, when accuracy is important, we recommend using the more sophisticated model A_1 .

We also evaluated the number density of potential guide stars across the sky using various catalogs. Our findings confirmed that the XGBOOST catalog, which contains spectroscopic parameters based on BP/RP spectra, provides a sufficient number of bright stars, suitable for guiding purposes across the vast majority of the sky, even with stringent selection criteria for low extinction. This ensures that the Roman mission will have a reliable supply of guide stars for its fine guidance system.

In conclusion, the new analytical models presented in this document provide a significant improvement in the ability to predict Roman magnitudes. These formulas, which are dependent on key stellar properties, offer a more precise method for selecting guide stars and estimating their flux. We note that commissioning will be the first real test of the accuracy of our algorithms and we will work to improve them if necessary when the first guide window data is taken. While this work is crucial for the Roman's guiding system, the developed models are also highly valuable for a broader range of astronomical studies. The models can be applied to both synthetic and real star catalogs, such as those from *Gaia* and 2MASS, thereby supporting a variety of simulations and scientific investigations that require accurate Roman magnitudes. The Python code for our implementation has been made publicly available to facilitate its use by the wider scientific community.

REFERENCES

- Aihara, H., Allende Prieto, C., An, D., et al. 2011, ApJS, 193, 29, doi: [10.1088/0067-0049/193/2/29](https://doi.org/10.1088/0067-0049/193/2/29)
- Allard, F., Homeier, D., & Freytag, B. 2012, Philosophical Transactions of the Royal Society of London Series A, 370, 2765, doi: [10.1098/rsta.2011.0269](https://doi.org/10.1098/rsta.2011.0269)
- Andrae, R., Rix, H.-W., & Chandra, V. 2023a, ApJS, 267, 8, doi: [10.3847/1538-4365/acd53e](https://doi.org/10.3847/1538-4365/acd53e)
- Andrae, R., Fouesneau, M., Sordo, R., et al. 2023b, A&A, 674, A27, doi: [10.1051/0004-6361/202243462](https://doi.org/10.1051/0004-6361/202243462)
- De Angeli, F., Weiler, M., Montegriffo, P., et al. 2023, A&A, 674, A2, doi: [10.1051/0004-6361/202243680](https://doi.org/10.1051/0004-6361/202243680)
- Flewelling, H. A., Magnier, E. A., Chambers, K. C., et al. 2020, ApJS, 251, 7, doi: [10.3847/1538-4365/abb82d](https://doi.org/10.3847/1538-4365/abb82d)
- Gaia Collaboration, Vallenari, A., Brown, A. G. A., et al. 2023, A&A, 674, A1, doi: [10.1051/0004-6361/202243940](https://doi.org/10.1051/0004-6361/202243940)
- Henden, A. A., Levine, S., Terrell, D., & Welch, D. L. 2015, in American Astronomical Society Meeting Abstracts, Vol. 225, American Astronomical Society Meeting Abstracts #225, 336.16

- Katz, D., Sartoretti, P., Guerrier, A., et al. 2023, A&A, 674, A5, doi: [10.1051/0004-6361/202244220](https://doi.org/10.1051/0004-6361/202244220)
- Lasker, B. M., Lattanzi, M. G., McLean, B. J., et al. 2008, AJ, 136, 735, doi: [10.1088/0004-6256/136/2/735](https://doi.org/10.1088/0004-6256/136/2/735)
- Marigo, P., Girardi, L., Bressan, A., et al. 2017, ApJ, 835, 77, doi: [10.3847/1538-4357/835/1/77](https://doi.org/10.3847/1538-4357/835/1/77)
- Marocco, F., Eisenhardt, P. R. M., Fowler, J. W., et al. 2021, ApJS, 253, 8, doi: [10.3847/1538-4365/abd805](https://doi.org/10.3847/1538-4365/abd805)
- Reinhart, M. 2022, SOC Guide Star Request and Selection Process, Tech. Rep. Roman-STScI-000008, Space Telescope Science Institute
- . 2023, Roman SOC FGS Algorithms, Tech. Rep. Roman-STScI-000416, Space Telescope Science Institute
- Schlafly, E. F., Meisner, A. M., & Green, G. M. 2019, ApJS, 240, 30, doi: [10.3847/1538-4365/aafbea](https://doi.org/10.3847/1538-4365/aafbea)
- Skrutskie, M. F., Cutri, R. M., Stiening, R., et al. 2006, AJ, 131, 1163, doi: [10.1086/498708](https://doi.org/10.1086/498708)
- Zhang, X., Green, G. M., & Rix, H.-W. 2023, MNRAS, 524, 1855, doi: [10.1093/mnras/stad1941](https://doi.org/10.1093/mnras/stad1941)

5 APPENDIX

5.1 Suggested updates to guiding prescriptions of Reinhart (2023)

5.1.1 Estimating Count Rates

As the throughput curves of Roman’s optical elements have changed, the zero-points (Z_R) to use to convert an estimated apparent magnitude m_R to estimated FGS count rate α_R (in units of e^-s^{-1}) has also changed. The method for the conversion has not and thus still follows section 18 of Reinhart (2023) and is given by

$$\alpha_R = \text{Max} (10^{-0.4(m_R - Z_R)} + \sigma_{\alpha, \text{detector}}, \alpha_{\text{min}, R}) \quad (12)$$

The new values for Z_R can be found in Table 3 along with the standard deviation the detector-to-detector variation, σ_Z . The $\alpha_{\text{min}, R}$ is minimum count rate, and $\sigma_{\alpha, \text{detector}}$ is the detector noise that is injected by the WFI detector. Their values are kept same as before, with $\alpha_{\text{min}, R} = 200e^-s^{-1}$ and $\sigma_{\alpha, \text{detector}} = 14e^-s^{-1}$.

5.1.2 Estimating Bright and Faint Limits

For estimating the bright and faint magnitude limits for a candidate guide star, we propose making minimal changes to section 3 of Reinhart (2023). We suggest changing the fixed error constant to be dynamically set by the RMS error of the polynomial fitting (listed in Table 5) and the zero-point error across the detectors (listed in Table 3). The resulting equation would be

$$\text{ErrorConst} = 3 \times (\sigma_{\text{RMS, fit}} + \sigma_Z). \quad (13)$$

We note that this error will be less than the current 0.5 dex for nearly all bands and schemes listed above and will be insignificant when compared to *BrightMagOffset* and *FaintMagOffset* (defined as 2.0 dex). We hope that further ground testing and commissioning will allow us to decrease these offsets and have more constraining limits on the guide star candidate magnitudes in the future. However, to avoid unnecessary failures during these tests, we suggest they are kept for now.

5.2 Checking Interpolation Consistency

To confirm our interpolation table of AB magnitudes matches the results from performing photometry of individual stellar spectra, we synthesized 3000 stellar spectra randomly distributed throughout the bounds of our interpolation table. We performed photometry in all the Roman bandpasses and compared them to the interpolated values. [Figure 7](#) and [Figure 8](#) show the resulting magnitude residuals of the Roman bandpasses relative to the predicted Gaia RP magnitudes versus the models' metallicities. All of the residuals are small, with imaging filter residuals within 0.02 dex and the dispersive element residuals within 0.04 dex and with RMS values of < 0.002 dex. However the majority of the deviations arise directly on either side of the metallicity of the models that make up the Phoenix spectral suite (the model metallicity values are represented by the vertical dotted lines in [Figure 7](#) and [Figure 8](#)). Excluding these regions, where the interpolation across metallicity breaks down, the agreement is well within 0.005 dex for all the Roman bandpasses.

5.3 Tables of polynomial coefficients

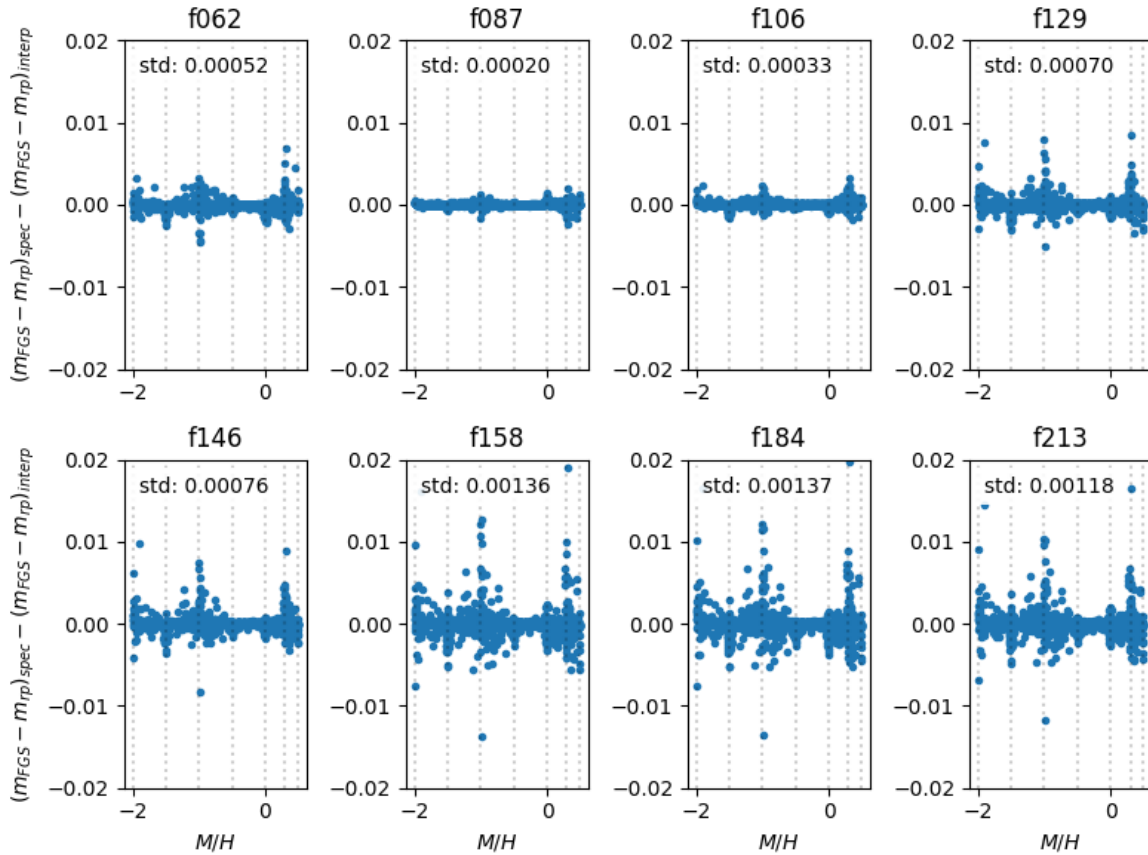


Figure 7: Residuals of AB magnitude difference from our interpolation table to interpolated stellar spectra for the Roman imaging filters. Vertical lines represent the metallicities of the models used to perform both interpolations.

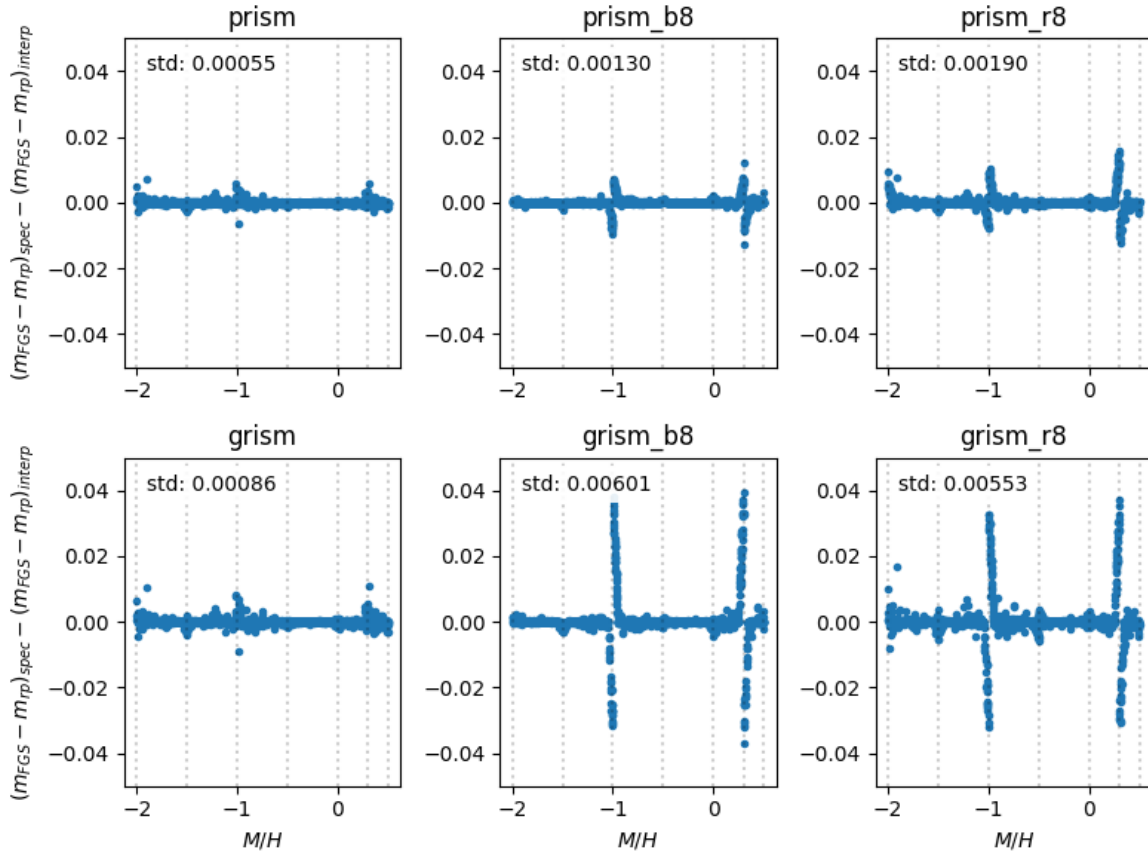


Figure 8: Residuals of AB magnitude difference from our interpolation table to interpolated stellar spectra for the Roman dispersive element photometry needed for guide star selection. Vertical lines represent the metallicities of the models used to perform both interpolations.

Table 7: Coefficient for estimating apparent magnitude in Roman bandpasses using Equation 5 and variables (G_{BP} , G_{RP} , A_G , $[M/H]$) from the GSC catalog (scheme A).

band	l	$c_{0,l}$	$c_{1,l}$	$c_{2,l}$	$c_{3,l}$	$c_{4,l}$	$c_{5,l}$	$c_{6,l}$	$c_{7,l}$	$c_{8,l}$
f062	giant	2.1443e-01	2.2406e-01	1.2538e-01	-1.0823e-02	2.7542e-04	-1.0698e-02	2.4599e-02	4.2490e-03	-1.8883e-02
f062	dwarf	6.9971e-02	6.4619e-01	-3.3106e-01	1.9284e-01	-3.1281e-02	-1.7547e-02	2.0961e-02	-1.1741e-02	-1.2907e-03
f062	none	1.7937e-01	2.7718e-01	9.7526e-02	-4.8688e-03	-1.8495e-04	-1.3936e-02	2.2331e-02	3.9563e-03	-1.7652e-02
f087	giant	4.0865e-01	-9.0465e-03	-1.3014e-01	2.9617e-02	-1.8606e-03	-1.7090e-03	-1.8018e-02	7.4665e-03	-1.5184e-02
f087	dwarf	5.8857e-01	-4.5032e-01	2.9215e-01	-1.3640e-01	1.9634e-02	5.1727e-03	-5.9534e-02	1.0434e-02	-8.8442e-03
f087	none	5.0294e-01	-1.6636e-01	-3.4172e-02	6.3195e-03	-4.7913e-05	1.4919e-03	-3.7586e-02	6.3608e-03	-7.2570e-03
f106	giant	6.6461e-01	-3.1936e-01	-1.1747e-01	2.7593e-02	-1.5514e-03	1.9867e-02	-2.4485e-02	1.6855e-02	-3.8064e-02
f106	dwarf	7.5058e-01	-3.7957e-01	-1.6384e-01	1.0554e-01	-2.3282e-02	3.1106e-02	-6.7556e-02	2.3596e-02	-4.1657e-02
f106	none	7.9475e-01	-5.1036e-01	-9.6512e-03	2.8938e-03	2.7855e-04	2.8974e-02	-4.8955e-02	1.6106e-02	-2.9394e-02
f129	giant	9.8735e-01	-7.1799e-01	-6.4932e-02	2.6439e-02	-1.5977e-03	4.0514e-02	2.2566e-02	2.6166e-02	-7.5062e-02
f129	dwarf	8.6085e-01	1.9830e-02	-1.0871e+00	5.9161e-01	-1.0421e-01	6.3404e-02	1.9665e-02	3.4048e-02	-1.0193e-01
f129	none	1.1485e+00	-9.2493e-01	3.6331e-02	6.2492e-03	-2.2804e-04	5.9192e-02	9.3296e-03	2.6896e-02	-7.2786e-02
f146	giant	1.1713e+00	-8.4516e-01	-8.4283e-02	3.8777e-02	-2.7450e-03	6.6896e-02	7.0205e-02	2.6396e-02	-8.8315e-02
f146	dwarf	8.7588e-01	3.2005e-01	-1.5069e+00	7.6732e-01	-1.2787e-01	7.8943e-02	3.6457e-02	2.9757e-02	-9.1327e-02
f146	none	1.2649e+00	-9.4187e-01	-4.0255e-02	3.0875e-02	-2.3219e-03	8.2497e-02	4.8781e-02	2.7604e-02	-8.4539e-02
f158	giant	1.4721e+00	-1.2559e+00	3.4257e-03	3.1030e-02	-2.3833e-03	9.7757e-02	1.2725e-01	3.2911e-02	-1.2084e-01
f158	dwarf	9.7214e-01	7.1224e-01	-2.4109e+00	1.2429e+00	-2.0537e-01	1.2368e-01	1.6284e-01	3.6118e-02	-1.5175e-01
f158	none	1.6131e+00	-1.3880e+00	4.1571e-02	2.9271e-02	-2.5838e-03	1.2374e-01	1.3370e-01	3.5758e-02	-1.2865e-01
f184	giant	1.8190e+00	-1.4405e+00	-1.4922e-02	4.3975e-02	-3.5362e-03	1.1029e-01	1.7615e-01	3.6202e-02	-1.4241e-01
f184	dwarf	1.1583e+00	1.0074e+00	-2.9341e+00	1.4840e+00	-2.4145e-01	1.3871e-01	1.9334e-01	3.6470e-02	-1.5877e-01
f184	none	1.9300e+00	-1.5106e+00	-1.3234e-02	5.0943e-02	-4.4548e-03	1.3969e-01	1.7823e-01	3.9738e-02	-1.5031e-01
f213	giant	2.0613e+00	-1.4044e+00	-5.0473e-02	4.9273e-02	-3.8033e-03	1.1130e-01	1.6070e-01	3.8248e-02	-1.4346e-01
f213	dwarf	1.4909e+00	7.3500e-01	-2.6136e+00	1.3262e+00	-2.1756e-01	1.2617e-01	1.5430e-01	4.0241e-02	-1.5275e-01
f213	none	2.1765e+00	-1.4925e+00	-3.1803e-02	5.0981e-02	-4.2772e-03	1.3476e-01	1.5322e-01	4.1058e-02	-1.4702e-01

Table 8: Coefficient for estimating apparent magnitude in Roman bandpasses (related to prism and grism) using Equation 5 and variables (G_{BP} , G_{RP} , A_G , [M/H]) from the GSC catalog (scheme A).

band	l	$c_{0,l}$	$c_{1,l}$	$c_{2,l}$	$c_{3,l}$	$c_{4,l}$	$c_{5,l}$	$c_{6,l}$	$c_{7,l}$	$c_{8,l}$
prism	giant	9.4260e-01	-6.0560e-01	-1.0765e-01	3.7400e-02	-2.5646e-03	4.8747e-02	3.8357e-02	2.0996e-02	-6.5647e-02
prism	dwarf	7.6720e-01	1.0887e-01	-9.8619e-01	4.9888e-01	-8.3934e-02	5.6119e-02	-1.3181e-02	2.4431e-02	-6.0861e-02
prism	none	1.0153e+00	-6.8957e-01	-6.0768e-02	2.6955e-02	-1.8707e-03	5.9360e-02	1.0106e-02	2.1442e-02	-5.8297e-02
grism	giant	1.1863e+00	-9.0082e-01	-6.2392e-02	3.4427e-02	-2.4111e-03	6.6972e-02	7.0624e-02	2.7704e-02	-9.1919e-02
grism	dwarf	8.8655e-01	3.3064e-01	-1.5926e+00	8.2194e-01	-1.3787e-01	8.4298e-02	5.6393e-02	3.2047e-02	-1.0529e-01
grism	none	1.3035e+00	-1.0273e+00	-7.7902e-03	2.5233e-02	-1.9204e-03	8.5412e-02	5.6177e-02	2.9121e-02	-9.0641e-02
prism_b8	giant	4.6516e-01	-7.7828e-02	-1.3133e-01	2.7137e-02	-1.5519e-03	6.6240e-03	-3.3058e-02	8.9019e-03	-1.4985e-02
prism_b8	dwarf	6.9334e-01	-6.3267e-01	3.7945e-01	-1.6535e-01	2.2035e-02	-6.6057e-04	-6.3344e-02	1.4644e-02	-1.8469e-02
prism_b8	none	5.8462e-01	-2.7946e-01	-1.0877e-02	-1.7377e-03	7.1124e-04	4.7210e-03	-5.0078e-02	7.7099e-03	-7.6512e-03
prism_r8	giant	1.0180e+00	-7.6944e-01	-4.5986e-02	2.2925e-02	-1.3515e-03	3.9194e-02	2.3733e-02	2.6726e-02	-7.6941e-02
prism_r8	dwarf	9.1175e-01	-5.4708e-02	-1.0909e+00	6.2001e-01	-1.1169e-01	5.0140e-02	4.9089e-02	3.8270e-02	-1.2439e-01
prism_r8	none	1.1964e+00	-1.0042e+00	6.8486e-02	1.7075e-04	2.3162e-04	5.4063e-02	1.6942e-02	2.7844e-02	-7.7408e-02
grism_b8	giant	7.1595e-01	-4.3025e-01	-6.1708e-02	1.5683e-02	-6.6740e-04	2.3739e-02	-2.3918e-02	1.7327e-02	-3.9812e-02
grism_b8	dwarf	7.1906e-01	-2.1844e-01	-3.9993e-01	2.2441e-01	-4.2800e-02	3.5511e-02	-5.7583e-02	2.2874e-02	-4.5037e-02
grism_b8	none	8.4783e-01	-6.0434e-01	2.6945e-02	-2.9465e-03	6.1070e-04	3.5652e-02	-4.3202e-02	1.6934e-02	-3.3309e-02
grism_r8	giant	1.7949e+00	-1.3823e+00	-4.7876e-02	5.1410e-02	-4.0887e-03	1.2725e-01	1.7205e-01	3.7330e-02	-1.4413e-01
grism_r8	dwarf	1.1335e+00	1.0380e+00	-2.9338e+00	1.4847e+00	-2.4261e-01	1.1585e-01	1.7100e-01	3.9805e-02	-1.5862e-01
grism_r8	none	1.9001e+00	-1.4558e+00	-3.5627e-02	5.4322e-02	-4.6326e-03	1.4233e-01	1.6353e-01	4.0644e-02	-1.4845e-01

Table 9: Coefficient for estimating apparent magnitude in Roman bandpasses using Equation 5 and variables (G_{BP}, G_{RP}) from the GSC catalog (scheme B_0). $c_{5,l}, c_{6,l}, c_{7,l}$, and $c_{8,l}$ are all 0 as in this scheme A_G and $[M/H]$ are unavailable.

band	l	$c_{0,l}$	$c_{1,l}$	$c_{2,l}$	$c_{3,l}$	$c_{4,l}$
f062	none	1.7116e-01	3.0045e-01	8.4891e-02	-3.9733e-03	-3.4576e-04
f087	none	4.6180e-01	-4.5151e-02	-1.5013e-01	3.7244e-02	-2.7668e-03
f106	none	7.0631e-01	-2.6156e-01	-2.3948e-01	6.2219e-02	-5.0079e-03
f129	none	1.0341e+00	-6.2022e-01	-2.2411e-01	6.8086e-02	-5.9348e-03
f146	none	1.1595e+00	-6.7478e-01	-2.5632e-01	7.8865e-02	-6.8761e-03
f158	none	1.4984e+00	-1.1197e+00	-1.4930e-01	6.4087e-02	-6.1885e-03
f184	none	1.8147e+00	-1.2516e+00	-1.8273e-01	7.6974e-02	-7.3995e-03
f213	none	2.0479e+00	-1.1905e+00	-2.4614e-01	8.9890e-02	-8.3284e-03
prism	none	9.2388e-01	-4.4972e-01	-2.6511e-01	7.5335e-02	-6.3393e-03
grism	none	1.1938e+00	-7.5022e-01	-2.3014e-01	7.4088e-02	-6.5770e-03
prism_b8	none	5.3232e-01	-1.2587e-01	-1.5853e-01	3.7834e-02	-2.7583e-03
prism_r8	none	1.0819e+00	-6.9866e-01	-1.9033e-01	6.0937e-02	-5.4063e-03
grism_b8	none	7.5633e-01	-3.4982e-01	-2.0592e-01	5.6606e-02	-4.7099e-03
grism_r8	none	1.7761e+00	-1.1706e+00	-2.3247e-01	8.8212e-02	-8.2527e-03

Table 10: Coefficient for estimating apparent magnitude in Roman bandpasses using Equation 5 and variables (J, K_s) from the GSC catalog (scheme C_0). $c_{5,l}, c_{6,l}, c_{7,l}$, and $c_{8,l}$ are all 0 as in this scheme A_G and $[M/H]$ are unavailable.

band	l	$c_{0,l}$	$c_{1,l}$	$c_{2,l}$	$c_{3,l}$	$c_{4,l}$
f062	none	2.9742e-01	3.5472e+00	-2.0504e+00	2.2812e+00	-5.7742e-01
f087	none	6.5073e-01	1.6182e+00	2.3265e-01	1.5348e-02	-2.0993e-02
f106	none	8.7183e-01	9.1887e-01	7.7837e-01	-5.4877e-01	1.1362e-01
f129	none	1.1222e+00	2.6033e-01	1.1228e+00	-8.2905e-01	1.7508e-01
f146	none	1.2163e+00	2.3063e-01	9.6456e-01	-7.7227e-01	1.7199e-01
f158	none	1.4532e+00	-4.1801e-01	1.2950e+00	-9.4153e-01	2.0034e-01
f184	none	1.7279e+00	-6.3557e-01	1.2823e+00	-9.9853e-01	2.2116e-01
f213	none	1.9905e+00	-7.1503e-01	1.4319e+00	-1.1823e+00	2.6785e-01
prism	none	1.0291e+00	6.4684e-01	7.4295e-01	-5.8633e-01	1.3008e-01
grism	none	1.2373e+00	1.0731e-01	1.0639e+00	-8.2001e-01	1.7881e-01
prism_b8	none	7.2633e-01	1.2994e+00	6.2349e-01	-3.2358e-01	5.7557e-02
prism_r8	none	1.1585e+00	1.2213e-01	1.2705e+00	-9.1192e-01	1.9073e-01
grism_b8	none	8.9272e-01	8.6040e-01	7.4342e-01	-4.9039e-01	9.5205e-02
grism_r8	none	1.7031e+00	-5.3202e-01	1.1731e+00	-9.6409e-01	2.1891e-01

Table 11: Coefficient for estimating apparent magnitude in Roman bandpasses using Equation 5 and variable G from the GSC catalog (scheme D_0). $c_{5,l}$, $c_{6,l}$, $c_{7,l}$, and $c_{8,l}$ are all 0 as in this scheme A_G and $[M/H]$ are unavailable.

band	l	$c_{0,l}$	$c_{1,l}$	$c_{2,l}$	$c_{3,l}$	$c_{4,l}$
f062	none	6.3737e+01	-2.4819e+01	3.8678e+00	-2.5429e-01	6.1983e-03
f087	none	-8.9943e+01	3.8584e+01	-5.8255e+00	3.9602e-01	-9.9772e-03
f106	none	-1.5010e+02	6.3511e+01	-9.6491e+00	6.5339e-01	-1.6400e-02
f129	none	-1.9194e+02	8.0984e+01	-1.2349e+01	8.3644e-01	-2.0999e-02
f146	none	-2.0314e+02	8.5707e+01	-1.3083e+01	8.8640e-01	-2.2259e-02
f158	none	-2.2980e+02	9.6947e+01	-1.4836e+01	1.0063e+00	-2.5296e-02
f184	none	-2.5239e+02	1.0645e+02	-1.6306e+01	1.1060e+00	-2.7800e-02
f213	none	-2.6488e+02	1.1168e+02	-1.7098e+01	1.1587e+00	-2.9102e-02
prism	none	-1.7644e+02	7.4545e+01	-1.1358e+01	7.6950e-01	-1.9322e-02
grism	none	-2.0648e+02	8.7107e+01	-1.3301e+01	9.0133e-01	-2.2637e-02
prism_b8	none	-1.0963e+02	4.6714e+01	-7.0686e+00	4.7945e-01	-1.2053e-02
prism_r8	none	-1.9422e+02	8.1948e+01	-1.2500e+01	8.4682e-01	-2.1263e-02
grism_b8	none	-1.5192e+02	6.4297e+01	-9.7756e+00	6.6231e-01	-1.6632e-02
grism_r8	none	-2.5397e+02	1.0708e+02	-1.6398e+01	1.1119e+00	-2.7942e-02